# HEAT FLUX DISTRIBUTION IN ASDEX UPGRADE - COMPARISON OF DIVERTOR I AND II

A. Herrmann, J.C.Fuchs, V.Rohde, M.Weinlich, ASDEX Upgrade team, NI-team, ICRH-team

*Max-Planck-Institut für Plasmaphysik, EURATOM Association, Garching; Germany*

## Introduction

In 1997, the open divertor of ASDEX Upgrade (DIV-I) was replaced by a new divertor (DIV-II) with a Lyra like shape of the inner and outer divertor plates and a roof baffle separating the inner and outer divertor leg. The strike point modules of DIV-II were hardened by use of carbon fibre composites to withstand heat fluxes of up to 15 MW/m$^2$ for 2 s [1]. This high heat fluxes were expected by conservatively extrapolating heat flux profiles measured in DIV-I to the DIV-II situation and taking into account the increased heating power of 25 MW coming into operation at ASDEX Upgrade in 1997.

Experiments without radiating mantle and a heating power up to 20 MW show that the DIV-II configuration results in a maximum heat flux of about 5 MW/m$^2$ at the outer strike point module. This value is well below the technical limitation of 10 MW/m$^2$ assumed for ITER divertor design.

In this paper we will present the poloidal distribution of energy load and heat flux in the Lyra shaped divertor of ASDEX Upgrade. Additionally, the scaling of peak load and heat flux decay lengths with plasma parameters derived for DIV-I of ASDEX Upgrade is compared with DIV-II.

## Diagnostics

Diagnostics were adapted to or installed in the DIV-II measuring the divertor load and the radiation losses.

The target load is measured by 3 thermography systems (Fig. 1). The closed geometry of the Lyra shaped divertor allows no direct view to the outer strike point module from outside the divertor region. To overcome this restriction a relay optics and a system of stainless steel mirrors installed inside the divertor slots is used to monitor the temperature at the strike point modules at one toroidal position. The existing thermography system [2] is used to measure the surface temperature of the retention and transition modules, as well as of the roof baffle. Both systems use the same type of an InSb IR line camera completed with a CAMAC based data acquisition system. The best time resolution is 130$\mu$s/line, the spatial resolution is about 1.2 mm/pixel at the strike point modules and varies between 2 mm and 8 mm for the other divertor modules. The heat flux to the different components is routinely calculated using the 2D-Code THEODOR [2]. In addition to the fast line cameras a 2D IR camera measuring at video frequency was installed to monitor the toroidal and poloidal temperature pattern at one section of the inner divertor.

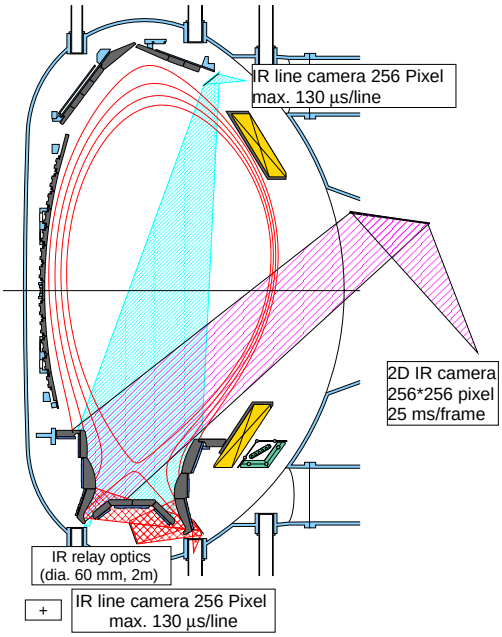


Fig. 1: Arrangement of IR cameras at ASDEX Upgrade.

The line integrals of radiation losses are measured with a set of 22 divertor bolometers and 72 bolometers in the main chamber. The time resolution of the bolometer systems is 1 ms. The measured line integral of radiation have been unfolded using the anisotropic diffusion model tomography [3] in order to reconstruct the radiation distribution in the divertor region as well as in the main chamber.

**Experimental results**

The experiments performed in ASDEX Upgrade covers a wide parameter range. In this paper we focus mainly to H-Mode discharges without radiation mantle which results in a maximum divertor power load at a given input power.

The poloidal distribution of the energy load to the divertor derived from thermographic measurements by temporal and spatial integration is shown in figure 2. The components of highest energy load are the roof baffle and the outer strike point module receiving about 30 % of the total divertor energy, each.

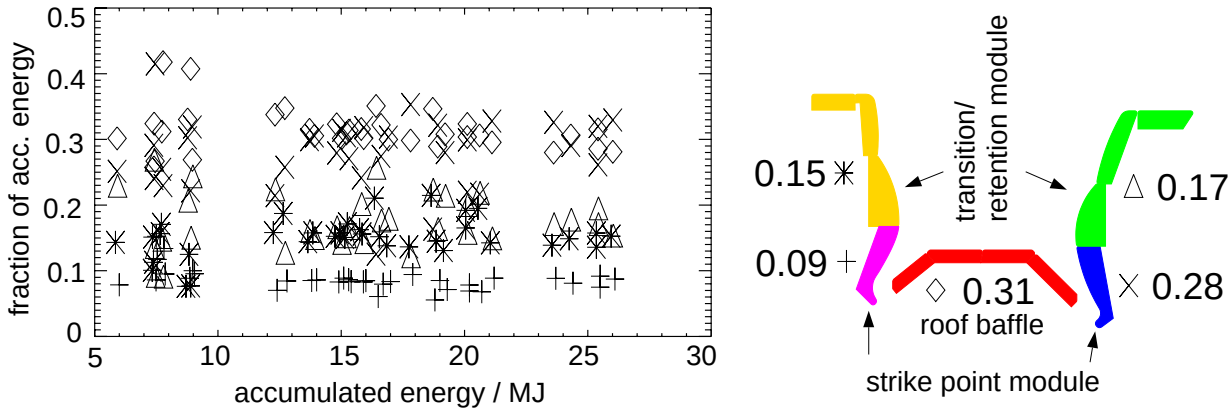


Fig. 2: (a) Energy accumulated by different divertor parts vs. shot accumulated energy (the meaning of the symbols is shown in (b)); (b) shot averaged accumulated energy for main divertor sections.

A typical heat flux profile for the DIV-II configuration shows a pronounced peak at the outer strike point region and a broad distribution with maximum heat fluxes below

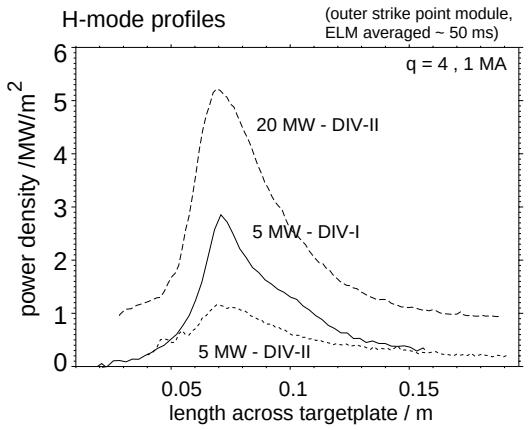


Fig. 3: Comparison of heat flux profiles measured in divertor-I and II at the outer target plate.

1 MW/m$^2$ for the other divertor modules [4].

In DIV-I as well as in DIV-II the maximum ELM averaged heat flux was found at the outer divertor plate. Figure 3 shows heat flux profiles across the outer divertor plates for DIV-I and DIV-II, respectively. The comparable profiles (5 MW input power) reveals that the maximum heat flux is reduced in DIV-II by about a factor of 3. The maximum heat flux measured in a high power (20 MW) discharge is only a factor 2 higher than the 5 MW DIV-I situation. This reduction in the maximum heat flux is not caused by simple geometric reasons. The conversion factor to calculate the parallel heat flux from the measured (projected) one (inverse angle of incidence) is shown in Fig. 4 for both geometries. These factors are com-

parable near to the position of maximum heat flux (32 and 40 for DIV-I and DIV-II, respectively). The radial variation of the conversion factor is minimized in DIV-II by optimizing the surface contour. But also in DIV-I the variation is less then 25 % over a distance of one heat flux decay length.

A set of H-mode heat flux profiles measured at the outer plate in DIV-I was used to find a dependence of the maximum heat flux and the decay length from global plasma parameters ($P_{plate}$, $q_{95}$, $\bar{n}_e$) [5].

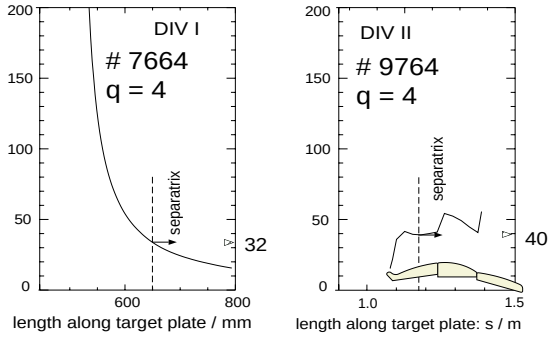


Fig. 4: Conversion factor to calculate the parallel heat flux for both divertor geometries.

A main result was, that the maximum heat flux as well as the decay length increase with the square root of the divertor power. A multi machine scaling reveals this behaviour also for other tokamaks [6].

The scaling derived for DIV-I applied to DIV-II data is shown in figures 5 and 6. The variation of discharge parameters used for DIV-II data points was as follows: $q_{95}$ = (3.4..5.6), $\bar{n}_e$ = (4...11)$\times 10^{19}$m$^{-3}$, $P_{sep}$ = (2...13) MW. It is obviously that the maximum heat flux and the decay length variation differs from the prediction. The same power law ansatz used for DIV-I was applied to DIV-II data. It results in the following dependence:

$$q_{max}\left(Wm^{-2}\right) \;=\; 0.114 P_{plate}^{1.10\pm0.06}(W)\; q_{95}^{1.6\pm0.6}\; \bar{n}_e^{-1.0\pm0.2}\left(10^{19}m^{-3}\right) \tag{1}$$

$$\lambda_p(m) \;=\; 0.34\; P_{plate}^{-0.07\pm0.06}(W)\; q_{95}^{-1.6\pm0.6}\; \bar{n}_e^{0.6\pm0.2}\left(10^{19}m^{-3}\right) \tag{2}$$

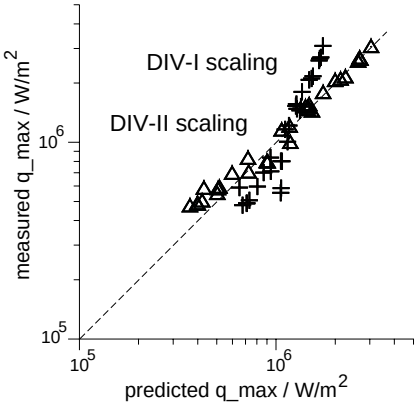


Fig. 5: Measured maximum heat flux in DIV-II vs. predicted maximum heat flux (plus - DIV-I, triangle - DIV-II).

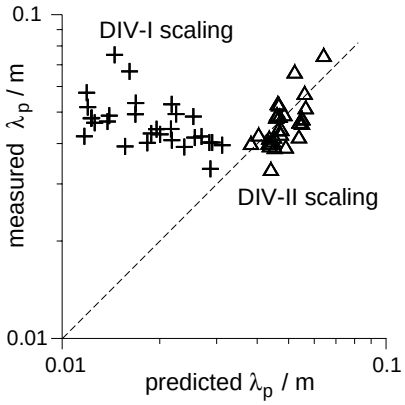


Fig. 6: Measured power decay length in DIV-II vs. predicted power decay length (plus - DIV-I, triangle - DIV-II).

The main difference between the DIV-I and DIV-II scaling is the dependence on the total divertor power (separatrix power) which is nearly linear for the maximum heat flux and independent for the decay length in DIV-II in contrast to a square root like dependence of both peak parameters in DIV-I.

## Discussion

The measured poloidal distribution of the energy load as well as the heat flux show that the lyra shaped divertor of ASDEX Upgrade allows an input power of 20 MW without reaching a critical value for divertor heat flux or energy accumulation. The higher power handling capacity of DIV-II compared to DIV-I is a benefit of the increased radiation losses in the divertor region. The fraction of power flowing into the divertor is about 50% of the input power for both divertor configurations. In DIV-I 50% - 60% of the power flowing into the divertor is lost by radiation. This value is increased to 70% - 80% in DIV-II. From this we expect that the heat flux to the divertor plates in DIV-II is reduced by a factor of 2 compared to DIV-I [4,7].

Though the fraction of energy transported to the divertor is the same for both divertors, the maximum heat flux is reduced by a factor of 2–3 (Fig. 3). This is caused by different detachment properties for both divertor configurations. Whereas DIV-I is a open divertor, DIV-II was optimized for neutral losses near to the separatrix region. This increases the radiation losses in the divertor and decreases the electron temperature. Due to the low electron temperatures the energy transport becomes convective and feeds a broader radial zone compared to conductive heat transport. A detailed discussion of the power loss mechanism in the divertor region is given in [8].

The higher level of detachment in DIV-II for comparable global plasma parameters results in the decreased maximum heat flux and the scaling found. It would be expected that high power discharges at low densities would decrease the level of detachment and would result in a heat flux to the outer divertor which is characterized by the DIV-I scaling.

## Summary

The heat flux to the Lyra shaped divertor of ASDEX Upgrade is reduced by a factor of 2–3 compared to DIV-I conditions due to increased radiation losses in the divertor region. The maximum ELM averaged heat flux is about 5 $MW/m^2$ for an input power of 20 MW (P/R = 15 MW/m).

## References

[1] IPP-Report IPP 1/281

[2] A. Herrmann, W. Junker, K. Günther et al., Plasma Phys. Control. Fusion 37 (1995) 17

[3] J.C. Fuchs, K.F. Mast, A. Herrmann et al., Contrib. 21st EPS (1994), 1308

[4] J.C. Fuchs, 'Radiation distribution and power balance in the ASDEX Upgrade LYRA divertor'; this conference,

[5] A. Herrmann, M. Laux, O. Kardaun et al., 23rd EPS conference on Contr. Fusion and Plasma Phys. II d039 (1996)

[6] A. Loarte, S. Bosch, A. Chankin et al., 'Multi machine scaling of the divertor peak heat flux and width for L-mode and H-mode discharges', to be published in J. of Nuc. Materials (PSI 1998).

[7] A. Herrmann, J.C. Fuchs, V. Rohde et al., 'Heat flux distribution in the divertor-II of ASDEX Upgrade', to be published in J. of Nuc. Materials (PSI 1998).

[8] R. Schneider, H.-S. Bosch, D. Coster et al., 'Role of divertor geometry on detachement and core plasma performance in ASDEX Upgrade', to be published in J. of Nuc. Materials (PSI 1998).